Several viewpoints have been adopted to study slow-fast systems, starting with asymptotic analysis [56, 164] using techniques such as matched asymptotic expansions [118, 148]. Geometric Singular Perturbation Theory (GSPT) takes a geometric point of view and focuses upon invariant manifolds, normal forms for singularities and analysis of their unfoldings [10, 69, 110, 111, 215]. Fenichel's seminal work [69] on invariant manifolds was an initial foundation of GSPT and it is also called Fenichel theory. A third viewpoint was adopted by a group of French mathematicians in Strasbourg. Using nonstandard analysis, they made many important discoveries [19, 20, 22, 23, 47, 48] about slow-fast systems. This paper adopts the GSPT viewpoint. We only focus on the results of GSPT that are necessary to study MMOs. There are other important techniques that are part of GSPT, such as the Exchange Lemma [110, 112], the blow-up method [55, 142, 233] and slow-fast normal form theory [10] that are not described in this paper.

2.1. The critical manifold and the slow flow. Solutions of a slow-fast system frequently exhibit slow and fast epochs characterized by the speed at which the solution advances. As $\varepsilon \to 0$, the trajectories of (2.1) converge during fast epochs to solutions of the *fast subsystem* or *layer equations*

$$\begin{cases} x' &= f(x,y,\lambda,0), \\ y' &= 0. \end{cases} \tag{2.3}$$

During slow epochs, on the other hand, trajectories of (2.2) converge to solutions of

$$\begin{cases} 0 &= f(x,y,\lambda,0), \\ \dot{y} &= g(x,y,\lambda,0), \end{cases} \tag{2.4}$$

which is a differential-algebraic equation (DAE) called the *slow flow* or *reduced system*. One goal of GSPT is to use the fast and slow subsystems, (2.3) and (2.4), to understand the dynamics of the full system (2.1) or (2.2) for $\varepsilon > 0$. The algebraic equation in (2.4) defines the *critical manifold*

$$S := \{(x,y) \in \mathbb{R}^m \times \mathbb{R}^n \mid f(x,y,\lambda,0) = 0\}.$$

We remark that S may have singularities [141], but we assume here that this does not happen so that S is a smooth manifold. The points of S are equilibrium points for the layer equations (2.3).

Fenichel theory [69] guarantees persistence of S (or a subset $M \subset S$) as a slow manifold of (2.1) or (2.2) for $\varepsilon > 0$ small enough if S (or M) is *normally hyperbolic*. The notion of normal hyperbolicity is defined for invariant manifolds more generally, effectively stating that the attraction to and/or repulsion from the manifold is stronger than the dynamics on the manifold itself; see [66, 67, 68, 95] for the exact definition. Normal hyperbolicity is often difficult to verify when there is only a single time scale. However, in our slow-fast setting, S consists entirely of equilibria and the requirement of normal hyperbolicity of $M \subset S$ is satisfied as soon as all $p \in M$ are hyperbolic equilibria of the layer equations, that is, the Jacobian $(D_x f)(p,\lambda,0)$ has no eigenvalues with zero real part. We call a normally hyperbolic subset $M \subset S$ *attracting* if all eigenvalues of $(D_x f)(p,\lambda,0)$ have negative real parts for $p \in M$; similarly M is called *repelling* if all eigenvalues have positive real parts. If M is normally hyperbolic and neither attracting nor repelling we say it is of *saddle type*.

Hyperbolicity of the layer equations fails at points on S where its projection onto the space of slow variables is singular. Generically, such points are folds in the sense of singularity theory [10]. At a fold point p_*, we have $f(p_*,\lambda,0) = 0$ and $(D_x f)(p_*,\lambda,0)$ has rank $m-1$ with left and right null vectors w and v, such that $w \cdot [(D^2_{xx} f)(p_*,\lambda,0)\,(v,v)] \neq 0$ and

$w \cdot [(D_y f)(p_*, \lambda, 0)] \neq 0$. The set of fold points forms a submanifold of codimension one in the n-dimensional critical manifold S. In particular, when $m = 1$ and $n = 2$, the fold points form smooth curves that separate attracting and repelling sheets of the two-dimensional critical manifold S. In this paper we do not consider more degenerate singular points of the projection of S onto the space of slow variables.

Away from fold points the implicit function theorem implies that S is locally the graph of a function $h(y) = x$. Then the reduced system (2.4) can be expressed as

$$\dot{y} = g(h(y), y, \lambda, 0). \tag{2.5}$$

We can also keep the DAE structure and write (2.4) as the restriction to S of the vector field

$$\left\{ \begin{array}{rcl} \dot{x} & = & -\left(D_x f\right)^{-1} \left(D_y f\right) g, \\ \dot{y} & = & g, \end{array} \right. \tag{2.6}$$

on $\mathbb{R}^m \times \mathbb{R}^n$ by observing that $f = 0$ and $\dot{y} = g$ imply $\dot{x} = -\left(D_x f\right)^{-1} \left(D_y f\right) g$. The vector field (2.6) blows up when f is singular. It can be *desingularized* by scaling time by $-\det\left(D_x f\right)$, at the expense of changing the direction of the flow in the region where this determinant is positive. This desingularized system plays a prominent role in much of our analysis. If S is normally hyperbolic, not only S, but also the slow flow on S persists for $\varepsilon > 0$; this is made precise in the following fundamental theorem.

THEOREM 2.1 (Fenichel's Theorem [69]). *Suppose $M = M_0$ is a compact normally hyperbolic submanifold (possibly with boundary) of the critical manifold S of* (2.2) *and that $f, g \in C^r$, $r < \infty$. Then for $\varepsilon > 0$ sufficiently small the following holds:*

- *(F1) There exists a locally invariant manifold M_ε diffeomorphic to M_0. Local invariance means that M_ε can have boundaries through which trajectories enter or leave.*
- *(F2) M_ε has a Hausdorff distance of $O(\varepsilon)$ from M_0.*
- *(F3) The flow on M_ε converges to the slow flow as $\varepsilon \to 0$.*
- *(F4) M_ε is C^r-smooth.*
- *(F5) M_ε is normally hyperbolic and has the same stability properties with respect to the fast variables as M_0 (attracting, repelling or saddle type).*
- *(F6) M_ε is usually not unique. In regions that remain at a fixed distance from the boundary of M_ε, all manifolds satisfying (F1)–(F5) lie at a Hausdorff distance $O(e^{-K/\varepsilon})$ from each other for some $K > 0$ with $K = O(1)$.*

The normally hyperbolic manifold M_0 has associated local stable and unstable manifolds

$$W^s_{\rm loc}(M_0) = \bigcup_{p \in M_0} W^s_{\rm loc}(p), \qquad \textit{and} \qquad W^u_{\rm loc}(M_0) = \bigcup_{p \in M_0} W^u_{\rm loc}(p),$$

where $W^s_{\rm loc}(p)$ and $W^u_{\rm loc}(p)$ are the local stable and unstable manifolds of p as a hyperbolic equilibrium of the layer equations, respectively. These manifolds also persist for $\varepsilon > 0$ sufficiently small: there exist local stable and unstable manifolds $W^s_{\rm loc}(M_\varepsilon)$ and $W^u_{\rm loc}(M_\varepsilon)$, respectively, for which conclusions (F1)–(F6) hold if we replace M_ε and M_0 by $W^s_{\rm loc}(M_\varepsilon)$ and $W^s_{\rm loc}(M_0)$ (or similarly by $W^u_{\rm loc}(M_\varepsilon)$ and $W^u_{\rm loc}(M_0)$).

We call M_ε a *Fenichel manifold*. Fenichel manifolds are a subclass of *slow manifolds*, invariant manifolds on which the vector field has speed that tends to 0 on the fast time scale as $\varepsilon \to 0$. We use the convention that objects in the singular limit have subscript 0, whereas the associated perturbed objects have subscripts ε.

2.1.1. The critical manifold and the slow flow in the Van der Pol equation. Let us illustrate these general concepts of GSPT with an example. One of the simplest systems in

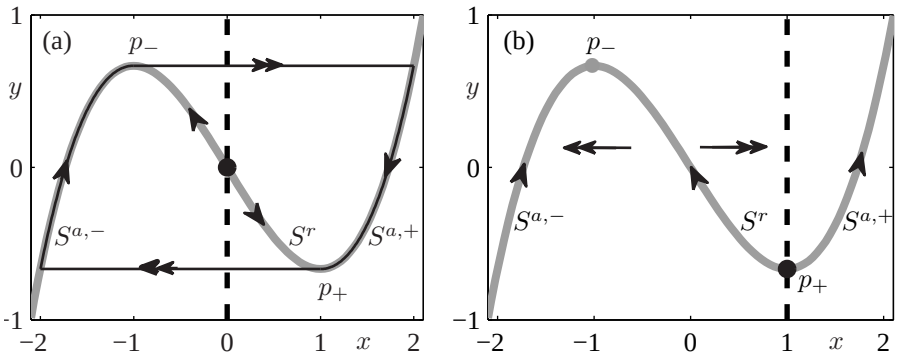

FIG. 2. *Phase portraits of the Van der Pol equation* (2.7) *for* $\lambda = 0$ *(a) and for* $\lambda = 1$ *(b). Shown are the critical manifold* S *(grey solid curve) and the* y*-nullcline (dashed line); double arrows indicate the direction of the fast flow and single arrows that of the slow flow. Panel (a) shows a candidate for a relaxation oscillation (black) surrounding an unstable equilibrium. Panel (b) is the moment of the singular Hopf bifurcation with a folded singularity at the local minimum* p_+.

which the concepts are manifest, and historically perhaps also the first, is the Van der Pol equation [222, 223, 224] with constant forcing $\lambda \in \mathbb{R}$ given by

$$\begin{cases} \varepsilon \dot{x} &= y - \frac{1}{3}x^3 + x, \\ \dot{y} &= \lambda - x. \end{cases} \tag{2.7}$$

This slow-fast system has only one fast and one slow variable, but it already exhibits complicated dynamics that were truly surprising when they were first discovered [48]. By setting $\varepsilon = 0$ in (2.7), we obtain the reduced system with an algebraic equation that defines the critical manifold of (2.7) as the cubic curve

$$S = \{(x, y) \in \mathbb{R}^2 \mid y = \tfrac{1}{3}x^3 - x =: c(x)\}. \tag{2.8}$$

It is normally hyperbolic away from the local maximum and minimum $p_\pm = (\pm 1, \mp\frac{2}{3})$ of the cubic, where S has a fold with respect to the fast variable x. At $p_\pm$ normal hyperbolicity fails, since $\frac{\partial}{\partial x} f(x, y, \lambda, 0) = 1 - x^2$ is zero at $p_\pm$. Hence, $p_\pm$ are the fold points and they naturally decompose the critical manifold into three branches,

$$S = S^{a,-} \cup \{p_-\} \cup S^r \cup \{p_+\} \cup S^{a,+},$$

where $S^{a,-} := S \cap \{x < -1\}$, $S^{a,+} := S \cap \{x > 1\}$ and $S^r = S \cap \{-1 < x < 1\}$. From the sign of $\frac{\partial}{\partial x} f(x, y, \lambda, 0)$ we conclude that the two branches $S^{a,-}$ and $S^{a,+}$ are attracting, and the branch S^r is repelling. The critical manifold S is shown as the grey cubic curve in Figure 2; note that S and its attracting/repelling nature does not depend on λ, so it is the same both in panel (a), where $\lambda = 0$, and panel (b), where $\lambda = 1$. The dynamics of any point not on S is entirely controlled by the direction of the fast variable x, which is indicated in Figure 2 by the horizontal double arrows; observe that the middle branch of S is repelling and the two unbounded branches are attracting.

To obtain the slow flow (2.5) on S in the Van der Pol equation (2.7) it is not actually necessary to solve the cubic equation $y = c(x)$ for x on $S^{a,-}$, S^r and $S^{a,+}$. It is more convenient to write the slow (reduced) flow in terms of the fast variable x. To this end, we differentiate $f(x, y, \lambda, 0) = y - c(x) = 0$ with respect to τ and obtain

$$\dot{y} = \dot{x}\, x^2 - \dot{x} = \dot{x}\,(x^2 - 1).$$

Combining this result with the equation for $\dot{y}$ we get:

$$(x^2 - 1)\,\dot{x} = \lambda - x \qquad \text{or} \qquad \dot{x} = \frac{\lambda - x}{x^2 - 1}. \tag{2.9}$$

The direction of the slow flow on S is indicated in Figure 2 by the arrows on the grey curve; panel (a) is for $\lambda = 0$ and panel (b) for $\lambda = 1$. The slow flow does depend on λ, because the direction of the flow is partly determined by the location of the equilibrium at $x = \lambda$ on S. The slow flow is well defined on $S^{a,-}$, S^r and $S^{a,+}$, but not at $x = \pm 1$ (as long as $\lambda \neq \pm 1$). We can desingularize the slow flow near $x = \pm 1$ by rescaling time with the factor $(x^2 - 1)$. This gives the equation $\dot{x} = \lambda - x$ of the *desingularized flow*. Note that this time rescaling reverses the direction of time on the repelling branch S^r, so care must be taken when relating the phase portrait of the desingularized system to the phase portrait of the slow flow.

Let us now focus specifically on the case for $\lambda = 0$, shown in Figure 2(a), because it is representative for the range $|\lambda| < 1$. The y-nullcline of (2.7) is shown as the dashed black vertical line (the x-nullcline is S) and the origin is the only equilibrium, which is a source for this value of λ. The closed curve is a singular orbit composed of two fast trajectories starting at the two fold points $p_\pm$ concatenated with segments of S. Such continuous concatenations of trajectories of the layer equations and the slow flow are called *candidates* [20]. The singular orbit follows the slow flow on S to a fold point, then it *jumps*, that is, it makes a transition to a fast trajectory segment that flows to another branch of S. The same mechanism returns the singular orbit to the initial branch of S. It can be shown [142, 164] that the singular orbit perturbs for $\varepsilon > 0$ to a periodic orbit of the Van der Pol equation that lies $O(\varepsilon)$ close to this candidate. Van der Pol introduced the term *relaxation oscillation* to describe periodic orbits that alternate between epochs of slow and fast motion.

2.2. Singular Hopf bifurcation and canard explosion. The dynamics of slow-fast systems in the vicinity of points on the critical manifold where normal hyperbolicity is lost can be surprisingly complicated and nothing like what we know from systems with a single time scale. This section addresses the phenomenon known as a *canard explosion*, which occurs in planar slow-fast systems after a *singular Hopf bifurcation*. We discuss this first for the example of the Van der Pol equation (2.7).

2.2.1. Canard explosion in the Van der Pol equation. As mentioned above, the phase portrait in Figure 2(a) is representative for a range of λ-values. However, the phase portrait for $\lambda = 1$, shown in Figure 2(b), is degenerate. Linear stability analysis shows that for $\varepsilon > 0$ the unique equilibrium point $(x, y) = (\lambda, \frac{1}{3}\lambda^3 - \lambda)$ is a source for $|\lambda| < 1$, but a sink for $|\lambda| > 1$. Supercritical Hopf bifurcations occur at $\lambda_H = \pm 1$. The analysis of how the observed stable dynamics of the Van der Pol equation (2.7) changes with λ from a stable focus to relaxation oscillations when $\varepsilon > 0$ is small was a major development in the theory of slow-fast systems. Figure 3(a) shows the result of a numerical continuation in the parameter λ of the periodic orbit for $\varepsilon = 0.05$ that emerges from the Hopf bifurcation. Close to the Hopf bifurcation at $\lambda_H = 1.0$ the periodic orbit is small (cyan curve), as is to be expected. However, as λ decreases, the periodic orbit grows very rapidly, where it follows the repelling slow manifold S^r_ε for a long time. In fact, the values of λ for all orange orbits in Figure 3(a) are $\lambda \approx 0.993491$, that is, they agree to six decimal places. Note that we show the growing orbits only up to a characteristic intermediate size: the largest periodic orbit in Figure 3(a) just encompasses the fold point p_-. Upon further continuation in λ this periodic orbit continues to grow rapidly until it reaches the shape of a relaxation oscillation; compare with Figure 2(a).

The Hopf bifurcation at $\lambda_H = 1$ occurs when the equilibrium moves over the fold point p_+. It is called a singular Hopf bifurcation. The eigenvalues at the Hopf bifurcation have

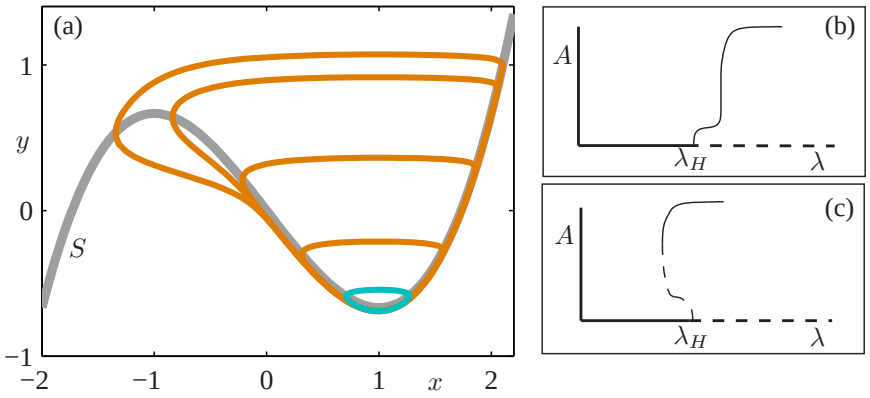

FIG. 3. *Numerical continuation of periodic orbits in the Van der Pol's equation* (2.7) *for* $\varepsilon = 0.05$. *Panel (a) shows a selection of periodic orbits: the cyan orbit is a typical small limit cycle near the Hopf bifurcation at* $\lambda = \lambda_H$, *whereas all the orange orbits occur in a very small parameter interval at* $\lambda \approx 0.993491$. *Panels (b) and (c) are sketched bifurcation diagrams corresponding to supercritical and subcritical singular Hopf bifurcations; here* A *denotes the amplitude of the limit cycle.*

magnitude $O(\varepsilon^{-1/2})$, so that the periodic orbit is born at the Hopf bifurcation with an intermediate period between the fast $O(\varepsilon^{-1})$ and slow $O(1)$ time scales. The size of this periodic orbit grows rapidly from diameter $O(\varepsilon^{1/2})$ to diameter $O(1)$ in an interval of parameter values λ of length $O(\exp(-K/\varepsilon))$ (for some $K > 0$ fixed) that is $O(\varepsilon)$ close to λ_H. Figures 3(b) and (c) are sketches of possible bifurcation diagrams in λ for the singular Hopf bifurcation in a supercritical case (which one finds in the Van der Pol system) and in a subcritical case, respectively; the vertical axis represents the maximal amplitude of the periodic orbits. The two bifurcation diagrams are sketches that highlight the features described above. There is a very small interval of λ where the amplitude of the oscillation grows in a square-root fashion, as is to be expected near a Hopf bifurcation. However, the amplitude then grows extremely rapidly until it reaches a plateau that corresponds to relaxation oscillations.

The rapid growth in amplitude of the periodic orbit near the Hopf bifurcation is called a *canard explosion*. The name canard derives originally from the fact that some periodic orbits during the canard explosion look a bit like a duck [48]. In fact, the largest periodic orbit in Figure 3(a) is an example of such a "duck-shaped" orbit. More generally, and irrespective of its actual shape, one now refers to a trajectory as a *canard orbit* if it follows a repelling slow manifold for a time of $O(1)$ on the slow time scale. A canard orbit is called a *maximal canard* if it joins attracting and repelling slow manifolds. Since the slow manifolds are not unique, this definition depends upon the selection of specific attracting and repelling slow manifolds; compare (F6) of Theorem 2.1. Other choices yield trajectories that are exponentially close to one another. In the Van der Pol equation (2.7) the canard explosion occurs $O(e^{-K/\varepsilon})$-close in parameter space to the point where the manifolds $S^{a,+}_\varepsilon$ and S^r_ε intersect in a maximal canard. It is associated with the parameter value $\lambda = 1$ where the equilibrium lies at the fold point p_+ of the critical manifold S; see Figure 2(b).

2.3. Singular Hopf bifurcation and canard explosion in generic planar systems. In the Van der Pol equation (2.7) the singular Hopf bifurcation takes place at $\lambda = 1$ where the equilibrium lies at a fold point. In a generic family of slow-fast planar systems a singular Hopf bifurcation does not happen exactly at a fold point, but at a distance $O(\varepsilon)$ in both phase space and parameter space from the coincidence of the equilibrium and fold point. One can

obtain a generic family by modifying the slow equation of the Van der Pol equation (2.7) to

$$\dot{y} = \lambda - x + a\, y.$$

In this modified system the equilibrium and fold point still coincide at $x = 1$, but the Hopf bifurcation occurs for $x = \sqrt{1 + \varepsilon\, a}$. A detailed dynamical analysis of canard explosion and the associated singular Hopf bifurcation using geometric or asymptotic methods exists for planar slow-fast systems [12, 13, 55, 56, 140, 142]; we summarize these results as follows.

THEOREM 2.2 (Canard Explosion in $\mathbb{R}^2$ [142]). *Suppose a planar slow-fast system has a generic fold point $p_* = (x_p, y_p) \in S$, that is,*

$$f(p_*, \lambda, 0) = 0, \quad \frac{\partial}{\partial x} f(p_*, \lambda, 0) = 0, \quad \frac{\partial^2}{\partial x^2} f(p_*, \lambda, 0) \neq 0, \quad \frac{\partial}{\partial y} f(p_*, \lambda, 0) \neq 0. \tag{2.10}$$

Assume the critical manifold is locally attracting for $x < x_p$ and repelling for $x > x_p$ and there exists a folded singularity for $\lambda = 0$ at p_*, namely,

$$g(p_*, 0, 0) = 0, \quad \frac{\partial}{\partial x} g(p_*, 0, 0) \neq 0, \quad \frac{\partial}{\partial \lambda} g(p_*, 0, 0) \neq 0. \tag{2.11}$$

Then a singular Hopf bifurcation and a canard explosion occur at

$$\lambda_H = H_1\, \varepsilon + O(\varepsilon^{3/2}) \qquad \textit{and} \tag{2.12}$$

$$\lambda_c = (H_1 + K_1)\, \varepsilon + O(\varepsilon^{3/2}). \tag{2.13}$$

The coefficients H_1 and K_1 can be calculated explicitly from normal form transformations [142] or by considering the first Lyapunov coefficient of the Hopf bifurcation [144].

In the singular limit we have $\lambda_H = \lambda_c$. For any $\varepsilon > 0$ sufficiently small, the linearized system [88, 147] at the Hopf bifurcation point has a pair of *singular eigenvalues* [27]

$$\sigma(\lambda; \varepsilon) = \alpha(\lambda; \varepsilon) + i\, \beta(\lambda; \varepsilon),$$

with $\alpha(\lambda_H; \varepsilon) = 0$, $\frac{\partial}{\partial \lambda} \alpha(\lambda_H; \varepsilon) \neq 0$ and

$$\begin{aligned} \lim_{\varepsilon \to 0} \beta(\lambda_H; \varepsilon) &= \infty, \quad \text{on the slow time scale } \tau, \quad \text{and} \\ \lim_{\varepsilon \to 0} \beta(\lambda_H; \varepsilon) &= 0, \quad \text{on the fast time scale } t. \end{aligned}$$

2.4. Folded singularities in systems with one fast and two slow variables. A canard explosion for a planar system happens in an exponentially small parameter interval. However, as soon as there is more than one slow variable, canard orbits can exist for $O(1)$ ranges of a parameter. To illustrate this, we consider (2.1) for the special case $m = 1$ and $n = 2$, and write it as

$$\left\{ \begin{array}{rcl} \varepsilon\, \dot{x} &=& f(x, y, \lambda, \varepsilon), \\ \dot{y}_1 &=& g_1(x, y, \lambda, \varepsilon), \\ \dot{y}_2 &=& g_2(x, y, \lambda, \varepsilon). \end{array} \right. \tag{2.14}$$

We assume that the critical manifold $S = \{f = 0\}$ of (2.14) has an attracting sheet S^a and a repelling sheet S^r that meet at a fold curve F as is shown in Figure 4. We also assume that the fold points $p_* \in F$ on S are generic in the sense of singularity theory, that is,

$$\begin{aligned} f(p_*, \lambda, 0) &= 0, \qquad \frac{\partial f}{\partial x}(p_*, \lambda, 0) &= 0, \\ \frac{\partial^2 f}{\partial x^2}(p_*, \lambda, 0) &\neq 0, \qquad D_y f(p_*, \lambda, 0) & \text{ has full rank one.} \end{aligned}$$

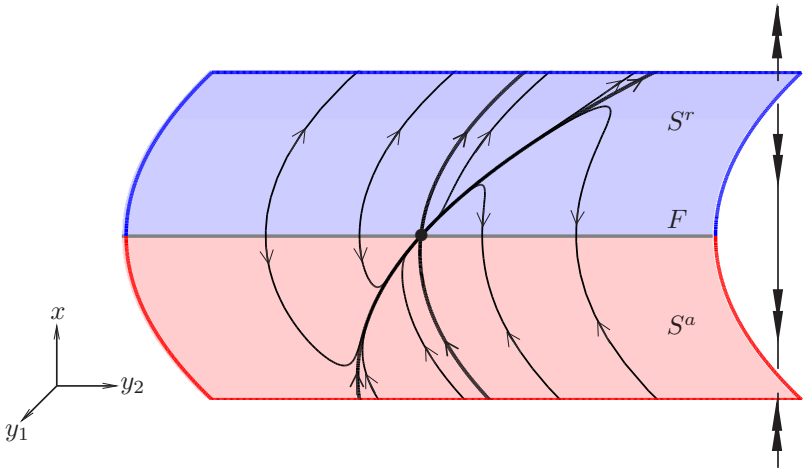

FIG. 4. *The critical manifold S with attracting sheet S^a (red) and repelling sheet S^r (blue) that meet at a fold curve F (grey). The fast flow transverse to S is indicated by double (large) arrows and the slow flow on S near a folded node by single (small) arrows; see also Figure 5(b).*

The slow flow is not defined on the fold curve before desingularization. At most fold points, trajectories approach or depart from both the attracting and repelling sheets of S. In generic systems, there may be isolated points, called *folded singularities*, where the trajectories of the slow flow switch from incoming to outgoing. Figure 4 shows an example of the slow flow on S and the thick dot on F is the folded singularity at which F changes from attracting to repelling (with respect to the slow flow).

Folded singularities are equilibrium points of the desingularized slow flow. As described above, the desingularized slow flow can be expressed as

$$\left\{\begin{array}{lcrcr} \dot{x} & = & \left(\frac{\partial}{\partial y_1} f\right)\, g_1 & + & \left(\frac{\partial}{\partial y_2} f\right)\, g_2\,, \\ \dot{y}_1 & = & & - & \left(\frac{\partial}{\partial x} f\right)\, g_1, \\ \dot{y}_2 & = & & - & \left(\frac{\partial}{\partial x} f\right)\, g_2, \end{array}\right. \tag{2.15}$$

restricted to S. A fold point $p_* \in F$ is a folded singularity if

$$g_1(p_*,\lambda,0)\,\frac{\partial f}{\partial y_1}(p_*,\lambda,0) + g_2(p_*,\lambda,0)\,\frac{\partial f}{\partial y_2}(p_*,\lambda,0) = 0.$$

There are different possibilities for the stability of p_* in (2.15). Let σ_1 and σ_2 denote the eigenvalues of the Jacobian matrix restricted to S and evaluated at a folded singularity p_*. We call p_* a

$$\left\{\begin{array}{lcll} \textit{folded saddle,} & \text{if} & \sigma_1\,\sigma_2 < 0, & \sigma_{1,2} \in \mathbb{R}, \\ \textit{folded node,} & \text{if} & \sigma_1\,\sigma_2 > 0, & \sigma_{1,2} \in \mathbb{R}, \\ \textit{folded focus,} & \text{if} & \sigma_1\,\sigma_2 > 0, & \mathrm{Im}(\sigma_{1,2}) \neq 0. \end{array}\right.$$

Figure 5 shows phase portraits of the (linearized) slow flow, in panels (a) and (b), and the associated desingularized slow flow, in panels (c) and (d), respectively. Panels (a) and (c) are for the case of a folded saddle and panels (b) and (d) of a folded node. For the case of a folded node one generically has an inequality of the form $|\sigma_1| > |\sigma_2|$, and we write $|\sigma_s| > |\sigma_w|$,

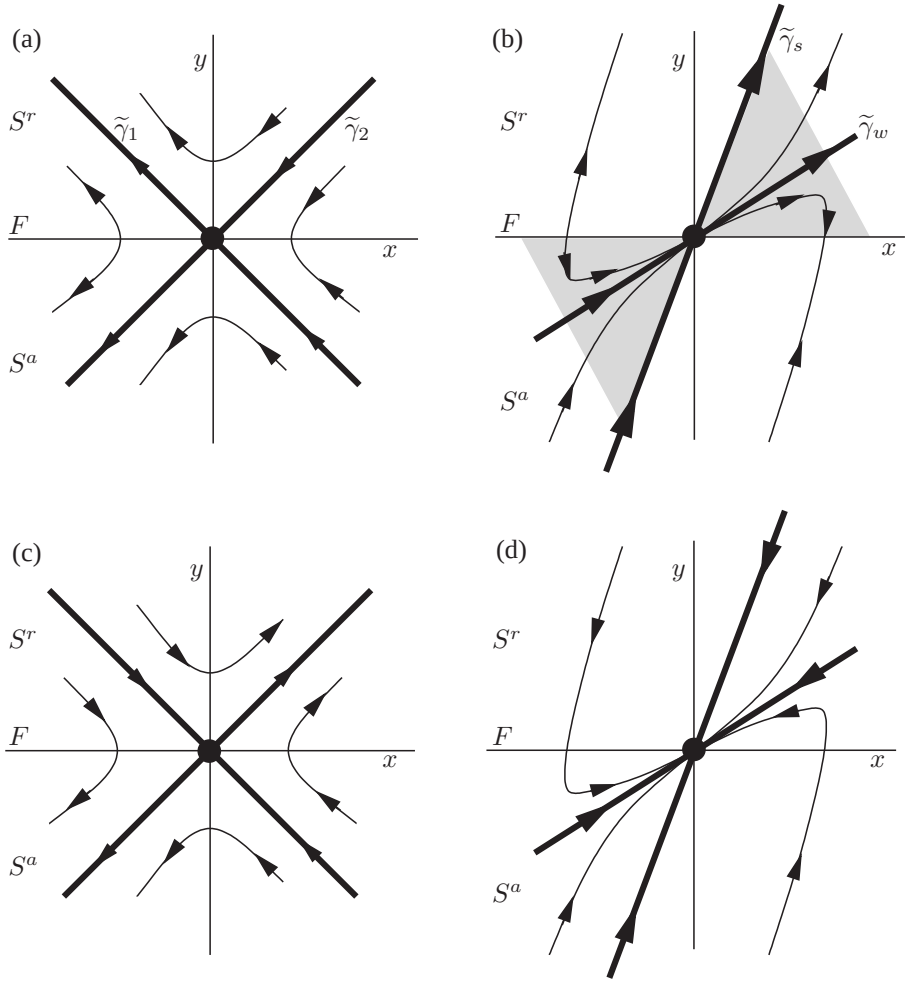

FIG. 5. *Phase portraits of the locally linearized slow flow near a folded saddle (a) and a folded node (b); the singular canards defined by the eigendirections are shown as thick lines. The corresponding desingularized slow flow is shown in panels (c) and (d), respectively.*

replacing the numeric labels with s and w to emphasize the strong and weak eigendirections. Note that the phase portraits for the slow flow in Figure 5(a) and (b) are obtained by reversing the direction of the flow on S^r where $\frac{\partial}{\partial x} f > 0$, that is, by reversing the arrows above F in the phase portraits of the desingularized slow flow in panels (c) and (d). It is an important observation that the trajectories of the slow flow that lie along the eigendirections of the folded saddle or node connect the two sheets of the critical manifold through the folded singularity in finite (slow) time; such a trajectory is called a *singular canard*. We remark that there are no singular canards for the case of a folded focus, which is why it is not shown here. Notice further for the case of the folded node in Figure 5(b) that the strong singular canard $\tilde{\gamma}_s$ and the fold curve bound a full (shaded) sector of trajectories that cross from S^a to S^r by passing through the folded node. The linearized system in Figure 5(b) should be compared with Figure 4, which shows a nonlinear slow flow near a folded node and, hence, also has a full sector of trajectories that pass through the folded singularity.

Singular canards act as candidates of maximal canards of the full system for $\varepsilon > 0$. This

is described in the next theorem [19, 23, 31, 212, 233].

THEOREM 2.3 (Canards in $\mathbb{R}^3$). *For the slow-fast system* (2.14) *with* $\varepsilon > 0$ *sufficiently small the following holds:*

(C1) There are no maximal canards generated by a folded focus.

(C2) For a folded saddle the two singular canards $\tilde{\gamma}_{1,2}$ *perturb to maximal canards* $\gamma_{1,2}$.

(C3.1) For a folded node let $\mu := \sigma_w/\sigma_s < 1$. *The singular canard* $\tilde{\gamma}_s$ *("the strong canard") always perturbs to a maximal canard* γ_s. *If* $\mu^{-1} \notin \mathbb{N}$ *then the singular canard* $\tilde{\gamma}_w$ *("the weak canard") also perturbs to a maximal canard* γ_w. *We call* γ_s *and* γ_w *primary canards.*

(C3.2) For a folded node suppose $k > 0$ *is an integer such that* $2k + 1 < \mu^{-1} < 2k + 3$ *and* $\mu^{-1} \neq 2(k + 1)$. *Then, in addition to* $\gamma_{s,w}$, *there are* k *other maximal canards, which we call secondary canards.*

(C3.3) The primary weak canard of a folded node undergoes a transcritical bifurcation for odd $\mu^{-1} \in \mathbb{N}$ *and a pitchfork bifurcation for even* $\mu^{-1} \in \mathbb{N}$.

3. Slow-fast mechanisms for MMOs. In this section we present key theoretical results of how MMOs arise in slow-fast systems with SAOs occurring in a localized region of the phase space. The LAOs, on the other hand, are associated with large excursions away from the localized region of SAOs. More specifically, we discuss four local mechanisms that give rise to such SAOs:

- passage near a folded node, discussed in Section 3.1;
- singular Hopf bifurcation, discussed in Section 3.2;
- three-time-scale problems with a singular Hopf bifurcation, discussed in Section 3.3;
- tourbillion, discussed in Section 3.4.

Each of these local mechanisms has its distinctive characteristics and can give rise to MMOs when combined with a *global return mechanism* that takes the trajectory back to the region with SAOs. Such global return mechanisms arise naturally in models from applications and a classic example is an S-shaped slow manifold; see Section 3.2 and the examples in Sections 4–6. We do not discuss global returns in detail, but rather concentrate on the nature of the local mechanisms. From the analysis of normal forms we estimate quantities that can be measured in examples of MMOs produced from both numerical simulations and experimental data. Specifically, we consider the number of SAOs and the changes in their amplitudes from cycle to cycle. We also consider in model systems the geometry of nearby slow manifolds that are associated with the approach to and departure from the SAO regions.

3.1. MMOs due to a folded node. Folded nodes are only defined for the singular limit (2.4) of system (2.1) on the slow time scale. However, they are directly relevant to MMOs because for $\varepsilon > 0$ small enough, trajectories of (2.1) that flow through a region where the reduced system has a folded node, undergo small oscillations. Benoit [19, 20] first recognized these oscillations. Wechselberger and collaborators [31, 212, 233] gave a detailed analysis of folded nodes while Guckenheimer and Haiduc [86] and Guckenheimer [84] computed intersections of slow manifolds near a folded node and maps along trajectories passing through these regions. From Theorem 2.3 we know that the eigenvalue ratio $0 < \mu < 1$ at the folded node is a crucial quantity that determines the dynamics in a neighborhood of the folded node. In particular, μ controls the maximal number of oscillations. The studies mentioned above use normal forms to describe the dynamics of oscillations near a folded node. Two equivalent versions of these normal forms are

$$\left\{ \begin{array}{rcl} \varepsilon\, \dot{x} &=& y - x^2, \\ \dot{y} &=& z - x, \\ \dot{z} &=& -\nu, \end{array} \right. \tag{3.1}$$